

Common packing patterns for jammed particles of different power size distributions

Daisuke S. Shimamoto¹* and Miho Yanagisawa¹†*Komaba Institute for Science, Graduate School of Arts and Sciences, The University of Tokyo, Komaba 3-8-1, Meguro, Tokyo 153-8902, Japan*

(Received 27 June 2022; accepted 12 January 2023; published 10 February 2023)

We introduce a model for particles that are extremely polydisperse in size compared with monodisperse and bidisperse systems. In two dimensions (2D), size polydispersity inhibits crystallization and increases the packing fraction at jamming points. However, no packing pattern common to diverse polydisperse particles has been reported. We focused on polydisperse particles with a power size distribution r^{-a} as a ubiquitous system that can be expected to be scale invariant. We experimentally and numerically constructed 2D random packing for various polydisperse particles with different size exponents a . Analysis of the packing pattern revealed a common contact number distribution for $a < 3$ and a higher jamming point for $2 < a < 3$ than in monodisperse systems. These findings demonstrate that the ambiguity of the characteristic length provides common properties that lead to a classification scheme for polydisperse particles.

DOI: [10.1103/PhysRevResearch.5.L012014](https://doi.org/10.1103/PhysRevResearch.5.L012014)

Polydisperse particles are omnipresent. Thermal particles, such as biomolecules in cells [1,2], and athermal particles, such as cement [3] and gravel [4–6], are highly dispersed in size and shape. Regarding size polydispersity, fracture-produced particles such as impact-fractured objects [7–9], fault gouge under tensile stress [4], and rubble by the collision of rock [6] have power size distribution. In addition, critical phenomena result in a power size distribution of the clusters. It is known that correlation lengths related to the cluster size cutoff diverge at the critical point and that the cluster size follows a power size distribution [10,11]. It is also known that droplets with a power-law distribution arise because of self-organized criticality [12,13]. Thus polydisperse particles with various power size distributions are ubiquitous and seemingly without any order; however, they have one thing in common: They have no apparent characteristic length.

In the context of jamming and glass transitions, such particle size dispersion has been considered based on monodisperse systems [14–20]. Previous studies have shown that size polydispersity suppresses crystallization at high packing fractions in two dimensions. Examples include bidisperse systems (size distribution with two peaks) with a size ratio of approximately 1.4 [15,21–24] and systems with a slight size dispersity around the average size [25–27]. In addition, more polydisperse bidisperse systems with larger size ratios

than 1.4 have been reported to exhibit unique phenomena, such as random packing at higher packing fractions [28,29] and the appearance of multiple glass phases [30,31]. Despite numerous experimental and numerical studies on polydisperse systems [3,15,21–25,28–35], there are no reports of common patterns to randomly packed polydisperse particles beyond the size polydispersity or of properties different from those of monodisperse particles.

Because we anticipate that scale invariance results in common patterns of jammed particles beyond the size polydispersity, we have concentrated on systems with power size distributions with no apparent characteristic lengths, such as the mean and standard deviation of the sizes.

We explored the random packing patterns and the jamming transitions by numerically and experimentally employing particles with various power size distributions, and we contrasted them with bidisperse systems. The power distribution of the particle radius has the minimum and maximum cutoffs at r_{\min} and r_{\max} . Although these r_{\min} and r_{\max} length scales exist due to constraints for physical realization, such as the finite number of particles and area, we have succeeded in deriving conditions under which these length scale effects can be neglected using experiments and simulations. Therefore this study contributes to describing the actual power size distribution, which can lead to practical scale invariance in jamming transitions.

Materials and methods. Distilled water (Ultra-Pure DNase/RNase-free distilled water; Invitrogen, Waltham, MA) with a surfactant Tween 20 (Sigma-Aldrich, St. Louis, MO) was used as a continuous phase. Mineral oil (Nacalai Tesque, Kyoto, Japan) with a surfactant, Span 80 (Tokyo Chemical Industry, Tokyo, Japan), was used as a dispersed phase. To facilitate identification of the oil-in-water (O/W) droplets, a lipophilic dye, capsanthin in vegetable oil (Tokyo Chemical Industry), was added to the mineral oil. The O/W droplets were prepared by using an aqueous solution containing 1 wt % Tween 20 and a mineral oil containing 0.1 wt % Span 80 and 2 wt % capsanthin oil.

*shimamoto-daisuke806@g.ecc.u-tokyo.ac.jp

†Also at Center for Complex Systems Biology, Universal Biology Institute, The University of Tokyo, Graduate School of Science, The University of Tokyo, Hongo 7-3-1, Bunkyo, Tokyo 113-0033, Japan; myanagisawa@g.ecc.u-tokyo.ac.jp

Published by the American Physical Society under the terms of the [Creative Commons Attribution 4.0 International license](https://creativecommons.org/licenses/by/4.0/). Further distribution of this work must maintain attribution to the author(s) and the published article's title, journal citation, and DOI.

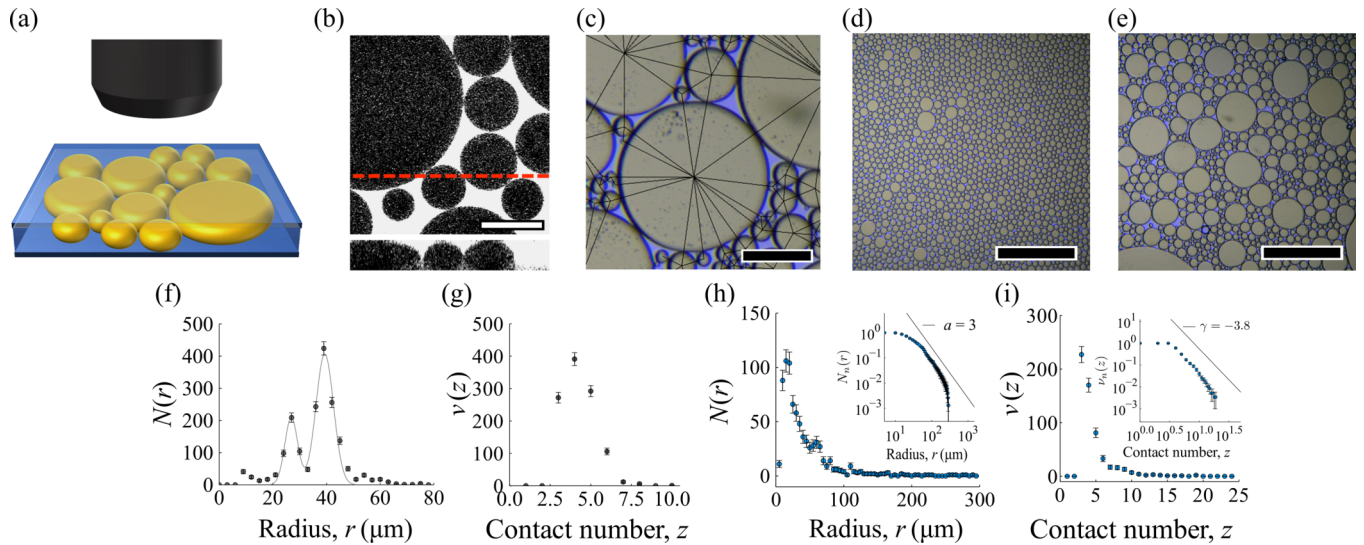


FIG. 1. (a) Schematic of the experimental setup of polydisperse droplets confined in 2D space. (b) Microscopic image of the polydisperse droplets from the top (top panel) and cross-sectional image along the dashed line in the top panel (bottom panel). The scale bar is $100\ \mu\text{m}$. (c) Micrograph of the packed droplets with the automatically detected contact lines. The scale bar is $200\ \mu\text{m}$. (d) and (e) Microscopic images for bidisperse and polydisperse systems, respectively. The scale bars are $1\ \text{mm}$. (f) and (g) Droplet radius distribution $N(r)$ and contact number distribution $\nu(z)$, respectively, for a bidisperse system. The solid curve in the $N(r)$ plot is the fitting line for multiple Gaussians, indicating that there are two peaks. (h) and (i) $N(r)$ and $\nu(z)$ for a polydisperse system. The inset log-log graphs show their normalized cumulative distributions, $N_n(r)$ and $\nu_n(z)$. (i) The radius distribution $N(r)$ follows a power size distribution of $a \simeq 3$ in the region of one order of magnitude.

To prepare monodisperse droplets, we used a centrifugal microfluidic device, which is a modified version of a previously reported device [36]. The device consists of three parts: a glass capillary, a micropipette tip (Labcon, Petaluma, CA), and a microtube. The glass capillary with a thin tip of $\sim 30\ \mu\text{m}$ and length of $8\ \text{mm}$ from the tip was fabricated from the ready-made capillary (outer diameter $1\ \text{mm}$, inner diameter $0.6\ \text{mm}$, G-1; Narishige, Tokyo, Japan) by using a puller (PC-10; Narishige) and microforge (MF-900; Narishige). The capillary was attached to the end of a micropipette tip ($200\text{-}\mu\text{l}$ standard yellow pipette tip). The micropipette tip was filled with $80\ \mu\text{l}$ of mineral oil and fixed on the microtube containing $500\ \mu\text{l}$ of the aqueous solution by passing through the 6-mm -diameter hole drilled in the lid of the microtube. The device was centrifuged at $6000\ \text{rpm}$ for $1\ \text{min}$ using a tabletop centrifuge (Wako Pure Chemical Industries, Osaka, Japan).

Polydisperse particles with a power size distribution were prepared by impact fracture of oil droplets in water. To the microtube containing $500\ \mu\text{l}$ aqueous solution, $150\ \mu\text{l}$ of mineral oil were added in three portions. Each time the oil was added, the microtube was tapped with a finger. Alternating the oil addition and tapping allows for the preparation of droplets with a power size distribution. The radii of the prepared droplets ranged from 14 to $421\ \mu\text{m}$.

To place the randomly packed particles in quasi-two-dimensional (quasi-2D) space, the O/W droplets were confined between two slide glasses ($76 \times 26\ \text{mm}$, thickness $\sim 0.9\ \text{mm}$, S1111; Matsunami, Osaka, Japan). These glasses were laminated together with $\sim 50\text{-}\mu\text{m}$ -thick double-sided tape to nearly match the diameter of the smallest droplet, $\sim 28\ \mu\text{m}$ [Fig. 1(a)]. To cover the glass surface with an

aqueous phase, the hydrophilicity of the glass slide surface was improved by using plasma cleaner (PDC-32G; Harrick Plasma, Ithaca, NY), which reduces the friction with the oil droplets. This quasi-2D confinement deforms the droplets into a flat pancake shape and eliminates overlap between droplets. Hence the center and edges of the droplet can be clearly identified. The water surrounding the droplet evaporates very slowly over time ($\sim 5\%/h$). This process increases the total area fraction occupied by the droplets (i.e., the packing fraction ϕ), while maintaining the area of each droplet. Here we determined the moment at the first avalanche that occurred as the jamming point and analyzed the packing pattern at that point. For the confirmation of the shape of the droplets, we took 3D images. Fluorescent molecules, $10\ \mu\text{M}$ TAMRA (Sigma-Aldrich), were added to the continuous phase to provide a clear distinction between the inside and the outside of the particles, and images were taken with a confocal microscope (FV1200; Olympus). The pancake shape of the particles and the realization of a 2D system were confirmed by 3D images [Fig. 1(b)].

Two-dimensional images of droplet packing were acquired using a camera (a2A5328-15ucPRO; Basler) attached to a microscope (SZX16; Olympus). The images were analyzed by using free National Institutes of Health (NIH) software, IMAGEJ [37]. The droplets in the images were detected by binarization after removing noise with a median filter and fast Fourier transform (FFT) bandpass filter. When the distance between the droplet surfaces was less than 1 pixel, the droplets were determined to be in contact with each other [Fig. 1(c)]. The automatically detected contacts were confirmed on the microscope image and were well matched, with an error of approximately 4% . As shown in the microscopic image of

Fig. 1(c), water outside the particle appears blue, while the particle surface with a large refractive index difference appears as a black ring. We judged that the particles were in contact if the black rings with neighboring droplets appeared to be connected without gaps in the confirmation.

Numerical calculations were performed by molecular dynamics simulations. The radii of the particles r were randomly set according to a given power size distribution r^{-a} using the inversion method. Exponent a was changed to a range $-5 < a < 10$, keeping the size range $r_{\max}/r_{\min} = 10^2$, where r_{\min} and r_{\max} are the lower and upper bounds of the distribution, respectively.

The packing was prepared by compression referring to some previous reports [31,38]. The particles have a repulsive potential U :

$$U = \frac{\epsilon}{2}(r_{ij} - D_{ij})^2 \Theta(r_{ij} - D_{ij}), \quad (1)$$

where D_{ij} is the distance between the i th and j th particles, r_{ij} is the sum of the radii of the i th and j th particles, and $\Theta(x) = 1$ for $x > 0$, otherwise $\Theta(x) = 0$. Initially, 4000 circular particles were randomly placed in a square space with side length L with periodic boundary conditions. The units of the length and the energy were set to be L and ϵ , respectively. Particles were relaxed to a local minimum of energy using the fast inertial relaxation engine (FIRE) algorithm [39]. Sufficient relaxation was determined to be completed when the maximum of the net force on each particle fell below 1.5×10^{-9} . While the pressure per particle after the relaxation, p , was lower than the certain value $p_{\text{thres}} = 10^{-5}$, the system was compressed by $\Delta\phi = 10^{-3}$ and relaxed repeatedly. In order to approach the jamming point, a method of compression and decompression [31] was employed. If p was higher than p_{thres} , the packing fraction was decreased by $\Delta\phi$. If it was lower, $\Delta\phi$ was multiplied by 0.5, and the packing fraction was increased by $\Delta\phi$. This procedure of compression and decompression was repeated until p was in the range of $\pm 2\%$ around p_{thres} .

Common pattern of packed particles. We analyzed the randomly packed particles with power size distribution r^{-a} in 2D at the jamming point and compared them with the bidisperse system. Figure 1(d) shows a microscopic image of the packing pattern of bidisperse droplets. The packing fraction was 0.85 ± 0.01 . To avoid crystallization, two differently sized particles were mixed. The ratio of the radii r was approximately 1 : 1.5. From this image, we calculated the distribution of the particle radius, $N(r)$, and the distribution of the contact number, $\nu(z)$, as shown in Figs. 1(f) and 1(g). The solid curve in Fig. 1(f) is the multiple-Gaussian fitting for $N(r)$, which shows that $N(r)$ has two peaks, a characteristic of a bidisperse system. During the analysis of the contact number z , particles with $z \leq 2$ (not included in the contact network) were successively removed as rattlers. The contact number distribution $\nu(z)$ has one peak, which seems to be Gaussian as suggested by previous work on bidisperse particles [40]. The average value is $\langle z \rangle \simeq 4.3$, which is similar to the ideal value $\langle z \rangle = 4$.

Similarly, the distributions of $N(r)$ and $\nu(z)$ for polydisperse particles were calculated from the microscopic images [Fig. 1(e)], where the packing fraction was 0.94 ± 0.02 . The

inset log-log plots of Figs. 1(h) and 1(i) show their normalized cumulative distributions, $N_n(r)$ and $\nu_n(z)$:

$$N_n(r) = \frac{\int_r^\infty N(r') dr'}{\int_0^\infty N(r') dr'}, \quad (2)$$

$$\nu_n(z) = \frac{\sum_z^\infty \nu(z')}{\sum_0^\infty \nu(z')}. \quad (3)$$

For this polydisperse system, $N(r)$ has a power size distribution of $a \simeq 3$ in the region of one order of magnitude, as shown in Fig. 1(h). The range of the power size distribution r_{\max}/r_{\min} is approximately 10, where r_{\min} and r_{\max} are the minimum and maximum cutoff lengths, respectively. The resulting average contact number was $\langle z \rangle \simeq 4.5$ [Fig. 1(i)]. On the other hand, the contact number distribution $\nu(z)$ also follows a power distribution $\nu(z) \propto z^{-\gamma}$, and not a Gaussian, but decayed more rapidly than $N(r)$ [see insets of Figs. 1(h) and 1(i)]. The exponent of $\nu(z)$ was found to be $\gamma \simeq 3.8$.

To investigate the generality of the contact number distribution for polydisperse systems, $\nu(z) \propto z^{-\gamma}$ with $\gamma \simeq 3.8$, suggested by the experiments, we numerically produced randomly packed patterns of various polydisperse particles with different a values. The particle size distributions are shown in Fig. 2. For $a = 1.5$ [Fig. 2(a)], r_{\max}/r_{\min} was set to 10^5 . This is because when a is small, the z distribution becomes too narrow, and many particles behave as rattlers. The cumulative distribution makes the cutoff r_{\max} affect regions with large r , resulting in a downward deviation of the plot.

Figure 3(a) shows examples of numerically produced packing patterns for $a = 1.5, 2, 2.5, 3,$ and 3.5 . For each a , the normalized cumulative contact number distributions $\nu_n(z)$ were calculated as plotted in Figs. 3(b)–3(f). Note that $\nu(z) = 0$ [$\nu_n(z) = 1$] for $z \leq 2$, because the rattlers were removed. Figures 3(b)–3(e) show that $\nu(z)$ for $a < 3$ follows a power-law distribution with $\gamma \simeq 3.8$ independent of a . This exponent agrees with the experimentally suggested value of $\gamma \simeq 3.8$ [Fig. 1(i)]. In addition, we have confirmed that $\langle z \rangle$ is approximately 4 regardless of a , same as that of the bidisperse system. These results demonstrate a common property for the contact number distribution of randomly packed polydisperse particles with $a < 3$. For a larger exponent ($a > 3$), deviation from the common power law was observed [Fig. 3(f)].

To explain the contact number distributions of $\nu(z) \propto z^{-\gamma}$ with constant $\gamma \simeq 3.8$ in $a < 3$, we modeled the system with dimension d with two assumptions: (i) If the particle size follows a power distribution, then the contact number also follows a power distribution $\nu(z) \propto z^{-\gamma}$ for $z \geq d + 1$ and $\nu(z) = 0$ for $z \leq d$, for all particles except rattlers are in contact with at least $d + 1$ particles. In general, $\nu(z)$ cannot be estimated from $r(z)$, but here we assume a power distribution. (ii) $\langle z \rangle = 2d$. This assumption is based on the fact that $\langle z \rangle$ is $2d$ at the jamming point, and is easily derived from Laman's theorem [41] when $d = 2$.

From assumption (ii), the following equality holds:

$$\langle z \rangle = \frac{\sum_{z=d+1}^\infty z \nu(z)}{\sum_{z=d+1}^\infty \nu(z)} = 2d. \quad (4)$$

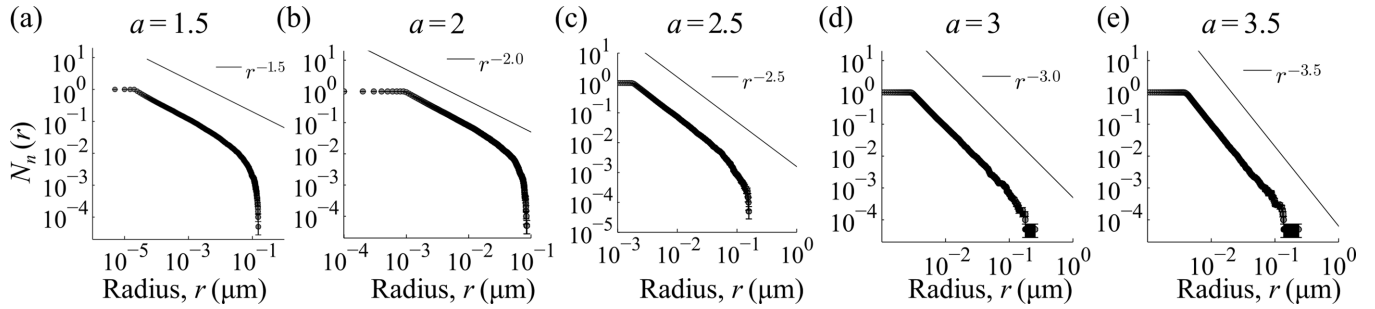


FIG. 2. Cumulative radius distribution $N(r)$ for numerically produced polydisperse systems, r^{-a} . (a), (b), (c), (d), and (e) $a = 1.5, 2, 2.5, 3,$ and $3.5,$ respectively. The error bars represent the standard deviation of five multiple runs.

For $d = 2,$ this can be expressed as follows using assumption (i):

$$\frac{\zeta(\gamma - 1, d + 1)}{\zeta(\gamma, d + 1)} = 4, \tag{5}$$

where $\zeta(z, a)$ denotes the Hurwitz zeta function. Solving Eq. (5) yields $\gamma = 3.83 \dots$ when $d = 2,$ which explains the property obtained experimentally and numerically (Figs. 1 and 3). The exponent $\gamma \simeq 3.8$ is considered sufficient as long as assumption (i) remains valid. This suggests that the assumption is not satisfied with $a > 3$ [Fig. 3(f)].

Classification of polydisperse systems from the jamming point. We identified that the common contact number distribution $\nu(z) \propto z^{-3.8}$ holds for $a < 3.$ To clarify the physical meaning of the range $a < 3$ and classification of such polydisperse systems, we investigated the jamming transitions for various polydisperse systems (Fig. 4). Pressure P was numerically calculated over a wide range, $-5 < a < 10,$ where the particles were compressed by a constant $\Delta\phi = 10^{-3}$ per step. Figure 4(a) suggests that the jamming point ϕ_c has a maximum value in the range $2 < a < 3.$ To precisely analyze

the a dependence of $\phi_c,$ we obtained ϕ_c with iteration of compression and decompression [31] [Fig. 4(b)]. For extremely small and large values of $a, a = -5$ and $a = 10,$ respectively, ϕ_c is close to the well-known value for bidisperse or small-dispersity systems of ~ 0.84 [22,26]. However, ϕ_c reaches a maximum value within the range $2 < a < 3.$ This means that the exponent range $2 < a < 3$ exhibits particularly strong characteristics of polydisperse systems.

Characteristic length in packing. We have shown that the contact number distributions have a common exponent 3.8 for $a < 3$ and a significantly higher packing fraction than the bidisperse system for $2 < a < 3.$ To explain the reason for this, here we discuss the implications of this range in terms of characteristic length scales: We examine the effect of the upper and lower limits of the particle size, i.e., r_{\max} and $r_{\min},$ on the packing pattern.

First, we consider the effect of $r_{\min},$ based on a comparison with an ideal system with $r_{\min} = 0.$ For $a < 3,$ the total area of particles under $r_{\min}, \int_0^{r_{\min}} \pi r^2 N(r) dr,$ can be made as small as desired by taking r_{\min} to be sufficiently small, which renders the effect of r_{\min} negligible. However, for $a > 3,$ the

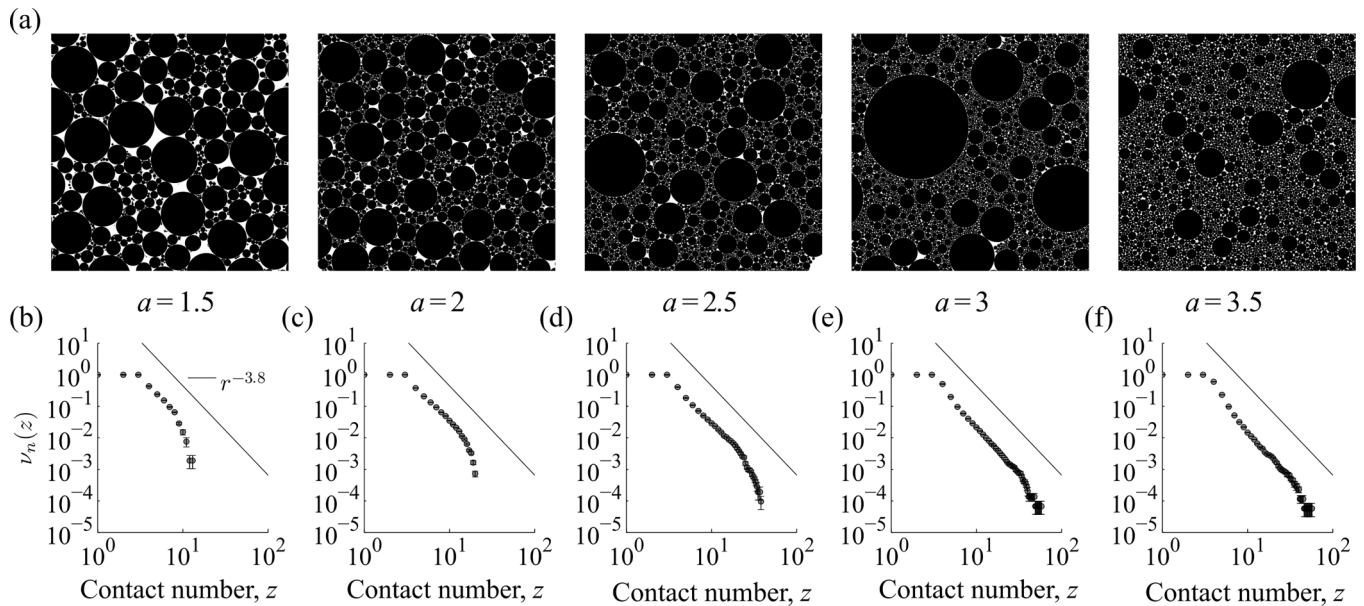


FIG. 3. (a) Examples of numerically produced packing patterns for various polydisperse systems r^{-a} and (b)–(f) corresponding normalized cumulative contact number distribution $\nu_n(z).$ For (b), (c), (d), (e), and (f), $a = 1.5, 2, 2.5, 3,$ and $3.5,$ respectively. The solid line indicates an exponent of 3.8. The error bars represent the standard deviation of five multiple runs.

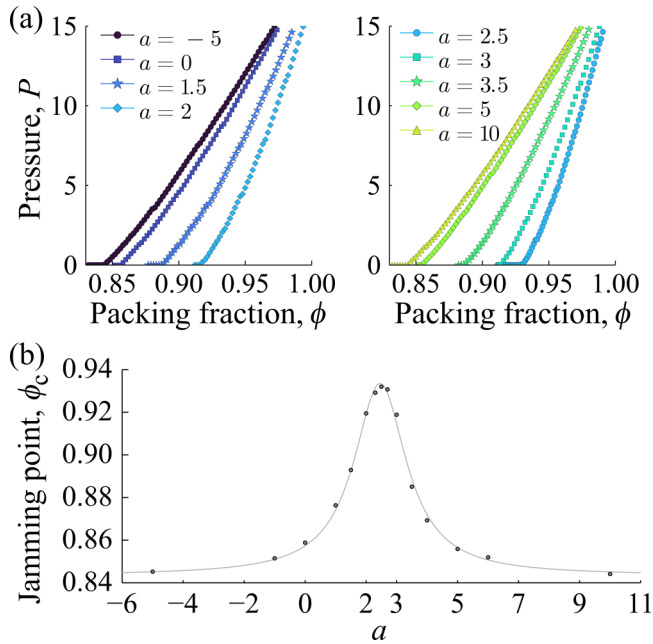


FIG. 4. (a) Dependence of pressure P on the packing fraction ϕ for various a . (b) Dependence of ϕ_c on a .

divergence of $\int_0^{r_{\max}} \pi r^2 N(r) dr$ makes the packing of particles with an ideal distribution undefinable. For the actual system, we must set a finite r_{\min} because the limit of $r_{\min} \rightarrow 0$ cannot be taken. This means that r_{\min} remains as the characteristic length for $a > 3$.

Next, we consider the effect of r_{\max} based on a comparison with complete packing, which is a packing without voids constructed by optimal arrangement. In a two-dimensional system, the minor numbers of small particles make complete packing impossible for $a < 2.3 \dots$. The condition of $a \simeq 2.3$ corresponds to Apollonian packing, which is a complete packing with the smallest a ($=d_A + 1$, where d_A is a fractal dimension of Apollonian packing) and the smallest number of particles [33,42]. Similarly, when a is too small for the random packing, the space around large particles is not sufficiently filled. The random packing contains voids in comparison to the optimally ordered Apollonian packing; yet it nevertheless achieves a packing fraction of 0.93, which is noticeably greater than the value of bidisperse systems, ~ 0.84 . Due to

the scarcity of small particles, large particles contact each other to form a pattern. Consequently, r_{\max} appears as the characteristic length.

Thus, for sufficiently large a , $a > 3$, a characteristic length r_{\min} emerges, and the scale-free nature is broken, which violates assumption (i). This is analogous to the absence of small-length cutoffs in fractal figures. Furthermore, both r_{\min} and r_{\max} have negligible effects on the pattern in the range $2 < a < 3$. This ambiguity in the characteristic length scale enhances the polydispersity and leads to a high packing fraction for polydisperse systems.

We have demonstrated that the packing of polydisperse particles with $N(r) \propto r^{-a}$ has a common property for the contact number distribution when the exponent a is smaller than 3. Furthermore, the power distribution with $2 < a < 3$ corresponds to the range in which a particularly strong polydispersity appears during the jamming transition. The proposed classification based on a may be applicable to various polydisperse systems with a power size distribution [6,43] and general probability distributions by generalizing a as follows:

$$a = -\frac{\ln N(r)}{\ln r}, \quad (6)$$

where $r \ll 1$.

Finally, we discuss how our findings contribute to the understanding and application of polydisperse systems. The scale-free nature of a polydisperse system may allow us to derive an exact solution of the jamming point ϕ_c at $r_{\min} \rightarrow 0$. In addition, when such polydisperse systems are at very high packing fraction beyond the jamming point, another common property may be derived from the analysis of particle dynamics and shape deformation. Furthermore, the condition $d_A + 1 < a < d + 1$, where the scale-free nature appears, will enhance the distinctive characteristics of polydisperse particles for general dimensions.

Acknowledgments. This research was funded by the Japan Society for the Promotion of Science (JSPS) KAKENHI (Grants No. 21H05871 and No. 22H01188) and Japan Science and Technology Agency (JST) program FOREST (Grant No. JPMJFR213Y). The authors thank Dr. Shio Inagaki (Kyushu University), Dr. Kyohei Takae (The University of Tokyo), Dr. Norihiro Oyama (Toyota Central R&D Labs, Inc.), and Yusuke Hara (The University of Tokyo).

[1] R. Phillips, J. Kondev, J. Theriot, H. G. Garcia, and N. Orme, *Physical Biology of the Cell* (Garland Science, London, 2012).
 [2] E. D. Kiehn and J. J. Holland, Membrane and nonmembrane proteins of mammalian cells. Synthesis, turnover, and size distribution, *Biochemistry* **9**, 1716 (1970).
 [3] F. W. Taylor and S. E. Thompson, *A Treatise on Concrete, Plain and Reinforced: Materials, Construction, and Design of Concrete and Reinforced Concrete* (Wiley, New York, 1909).
 [4] C. Sammis, G. King, and R. Biegel, The kinematics of gouge deformation, *Pure Appl. Geophys.* **125**, 777 (1987).

[5] R. D. Holtz, W. D. Kovacs, and T. C. Sheahan, *An Introduction to Geotechnical Engineering* (Prentice-Hall, Englewood Cliffs, NJ, 1981).
 [6] M. Grott, J. Biele, P. Michel, S. Sugita, S. Schröder, N. Sakatani, W. Neumann, S. Kameda, T. Michikami, and C. Honda, Macroporosity and grain density of rubble pile asteroid (162173) Ryugu, *J. Geophys. Res.: Planets* **125**, e2020JE006519 (2020).
 [7] L. Oddershede, P. Dimon, and J. Bohr, Self-Organized Criticality in Fragmenting, *Phys. Rev. Lett.* **71**, 3107 (1993).

- [8] T. Ishii and M. Matsushita, Fragmentation of long thin glass rods, *J. Phys. Soc. Jpn.* **61**, 3474 (1992).
- [9] H. Katsuragi, D. Sugino, and H. Honjo, Crossover of weighted mean fragment mass scaling in two-dimensional brittle fragmentation, *Phys. Rev. E* **70**, 065103(R) (2004).
- [10] C. Tang and P. Bak, Critical Exponents and Scaling Relations for Self-Organized Critical Phenomena, *Phys. Rev. Lett.* **60**, 2347 (1988).
- [11] X. Li, K. Hirose, T. Sakai, E. P. Gilbert, and M. Shibayama, SANS study on critical polymer clusters of tetra-functional polymers, *Macromolecules* **50**, 3655 (2017).
- [12] F. Family and P. Meakin, Scaling of the Droplet-Size Distribution in Vapor-Deposited Thin Films, *Phys. Rev. Lett.* **61**, 428 (1988).
- [13] L. Stricker, F. Grillo, E. A. Marquez, G. Panzarasa, K. Smith-Mannschott, and J. Vollmer, Universality of breath figures on two-dimensional surfaces: An experimental study, *Phys. Rev. Res.* **4**, L012019 (2022).
- [14] J. Bernal and J. Mason, Packing of spheres: Co-ordination of randomly packed spheres, *Nature (London)* **188**, 910 (1960).
- [15] C. S. O'Hern, L. E. Silbert, A. J. Liu, and S. R. Nagel, Jamming at zero temperature and zero applied stress: The epitome of disorder, *Phys. Rev. E* **68**, 011306 (2003).
- [16] M. van Hecke, Jamming of soft particles: Geometry, mechanics, scaling and isostaticity, *J. Phys.: Condens. Matter* **22**, 033101 (2010).
- [17] N. C. Karayiannis, K. Foteinopoulou, and M. Laso, The structure of random packings of freely jointed chains of tangent hard spheres, *J. Chem. Phys.* **130**, 164908 (2009).
- [18] A. J. Liu and S. R. Nagel, *Jamming and Rheology: Constrained Dynamics on Microscopic and Macroscopic Scales* (CRC, Boca Raton, FL, 2001).
- [19] P. Charbonneau, A. Ikeda, G. Parisi, and F. Zamponi, Glass Transition and Random Close Packing above Three Dimensions, *Phys. Rev. Lett.* **107**, 185702 (2011).
- [20] P. Charbonneau, E. I. Corwin, G. Parisi, and F. Zamponi, Universal Microstructure and Mechanical Stability of Jammed Packings, *Phys. Rev. Lett.* **109**, 205501 (2012).
- [21] W. Kob and H. C. Andersen, Testing mode-coupling theory for a supercooled binary Lennard-Jones mixture I: The van Hove correlation function, *Phys. Rev. E* **51**, 4626 (1995).
- [22] C. S. O'Hern, S. A. Langer, A. J. Liu, and S. R. Nagel, Random Packings of Frictionless Particles, *Phys. Rev. Lett.* **88**, 075507 (2002).
- [23] Z. Zhang, N. Xu, D. T. Chen, P. Yunker, A. M. Alsayed, K. B. Aptowicz, P. Habdas, A. J. Liu, S. R. Nagel, and A. G. Yodh, Thermal vestige of the zero-temperature jamming transition, *Nature (London)* **459**, 230 (2009).
- [24] N. Iikawa, M. M. Bandi, and H. Katsuragi, Sensitivity of Granular Force Chain Orientation to Disorder-Induced Metastable Relaxation, *Phys. Rev. Lett.* **116**, 128001 (2016).
- [25] D. J. Durian, Foam Mechanics at the Bubble Scale, *Phys. Rev. Lett.* **75**, 4780 (1995).
- [26] Y. Takehara and K. Okumura, High-Velocity Drag Friction in Granular Media near the Jamming Point, *Phys. Rev. Lett.* **112**, 148001 (2014).
- [27] N. Yanagisawa and R. Kurita, Size distribution dependence of collective relaxation dynamics in a two-dimensional wet foam, *Sci. Rep.* **11**, 2786 (2021).
- [28] S. Yerazunis, S. Cornell, and B. Wintner, Dense random packing of binary mixtures of spheres, *Nature (London)* **207**, 835 (1965).
- [29] J. Zheng, W. B. Carlson, and J. S. Reed, The packing density of binary powder mixtures, *J. Eur. Ceram. Soc.* **15**, 479 (1995).
- [30] H. Ikeda, K. Miyazaki, H. Yoshino, and A. Ikeda, Multiple glass transitions and higher-order replica symmetry breaking of binary mixtures, *Phys. Rev. E* **103**, 022613 (2021).
- [31] Y. Hara, H. Mizuno, and A. Ikeda, Phase transition in the binary mixture of jammed particles with large size dispersity, *Phys. Rev. Res.* **3**, 023091 (2021).
- [32] M. Hermes and M. Dijkstra, Jamming of polydisperse hard spheres: The effect of kinetic arrest, *Europhys. Lett.* **89**, 38005 (2010).
- [33] S. Kwok, R. Botet, A. Shglabov, and B. Cabane, Apollonian emulsions, *Europhys. Lett.* **130**, 38001 (2020).
- [34] C. Voivret, F. Radjai, J.-Y. Delenne, and M. S. El Youssoufi, Space-filling properties of polydisperse granular media, *Phys. Rev. E* **76**, 021301 (2007).
- [35] R. S. Farr and R. D. Groot, Close packing density of polydisperse hard spheres, *J. Chem. Phys.* **131**, 244104 (2009).
- [36] K. Maeda, H. Onoe, M. Takinoue, and S. Takeuchi, Controlled synthesis of 3D multi-compartmental particles with centrifuge-based microdroplet formation from a multi-barrelled capillary, *Adv. Mater.* **24**, 1340 (2012).
- [37] <https://imagej.nih.gov/ij/>.
- [38] H. Matsuyama, M. Toyoda, T. Kurahashi, A. Ikeda, T. Kawasaki, and K. Miyazaki, Geometrical properties of mechanically annealed systems near the jamming transition, *Eur. Phys. J. E* **44**, 133 (2021).
- [39] E. Bitzek, P. Koskinen, F. Gähler, M. Moseler, and P. Gumbsch, Structural Relaxation Made Simple, *Phys. Rev. Lett.* **97**, 170201 (2006).
- [40] P. Charbonneau, E. I. Corwin, G. Parisi, and F. Zamponi, Jamming Criticality Revealed by Removing Localized Buckling Excitations, *Phys. Rev. Lett.* **114**, 125504 (2015).
- [41] G. Laman, On graphs and rigidity of plane skeletal structures, *J. Eng. Math.* **4**, 331 (1970).
- [42] S. Manna and H. Herrmann, Precise determination of the fractal dimensions of Apollonian packing and space-filling bearings, *J. Phys. A* **24**, L481 (1991).
- [43] A. Meibom and I. Balslev, Composite Power Laws in Shock Fragmentation, *Phys. Rev. Lett.* **76**, 2492 (1996).